

Appropriate introduction of nitrile groups to balance NIR-II fluorescence imaging with photothermal therapy/photoacoustic imaging

Yaojun Li, Jingtao Ye, Yang Li, Minling Jiang, Tingyu Shi, Huayu Qiu, Shouchun Yin*

College of Material, Chemistry and Chemical Engineering, Hangzhou Normal University, Key Laboratory of Organosilicon Chemistry and Material Technology, Ministry of Education, Key Laboratory of Organosilicon Material Technology, Zhejiang Province, China

E-mail: yinsc@hznu.edu.cn

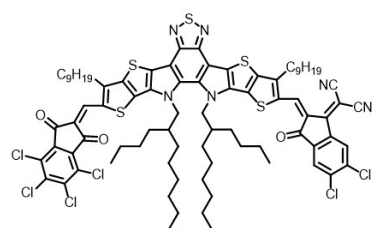
1. Materials and methods.....	S2
2. Synthetic procedures and characterization data	S2
2.1 Synthesis of BTP-TCID-2CN	S2
2.2 Synthesis of BTP-2TCID	S3
3. Theoretical calculation	S3
4. Fabrication and characteristic of nanoparticles	S3
5. Verification <i>J</i> -aggregation of BTP-2TCID NPs, BTP-TCID-2CN NPs and BTP-4CN NPs.....	S5
6. Photothermal performance of BTP-2TCID NPs, BTP-TCID-2CN NPs and BTP-4CN NPs.....	S5
7. Photodynamic properties of NPs	S7
8. Cell culture	S10
9. Intracellular uptake.....	S10
10. MTT assay	S10
11. ROS detection <i>in vitro</i>	S11
12. Live/dead cell staining assay	S12
13. Flow cytometry.....	S12
14. Animal model	S13
15. Photothermal imaging.....	S14
16. <i>In vitro</i> and <i>in vivo</i> fluorescence imaging	S14
17. <i>In vitro</i> and <i>in vivo</i> photoacoustic imaging	S14
18. <i>In vivo</i> anti-cancer therapy	S14
19. <i>In vivo</i> biological safe experiments	S15
20. Reference.....	S17

1. Materials and methods

¹H nuclear magnetic resonance (NMR) spectra were collected on a Bruker Advance 500 MHz spectrometer with CDCl₃ as deuterated solvent. Absorption spectra were performed on SHIMADZU UV-3600 plus spectrophotometer. The fluorescent emission spectra were conducted on an Edinburgh FLS 980 fluorescence spectrophotometer. Transmission electron microscopy (TEM) was performed on a Hitachi S-4800 and images were recorded on a Hitachi F-7700. Electron spin resonance (ESR) test was performed with JEOL JES-FA200. Photoacoustic imaging was detected using the multispectral optical tomography system (MSOT in Vision 256-TF, iThera Medical GmbH). Optical Fiber Coupler lasers (808 nm) were purchased from Ningbo Fingco Optoelectronic Co. Ltd. (Ningbo, China). Cellular fluorescence images were taken using a Nikon Eclipse 200 inverted fluorescence microscope and a BIO-RAD Radiance 2100 confocal laser scanning microscope (CLSM).

2. Synthetic procedures and characterization data

2.1 Synthesis of **BTP-TCID-2CN**



BTP-TCID-2CN was synthesized according to literature procedure.¹ ¹H NMR (500 MHz, CDCl₃, 298K) δ (ppm): 9.17 (s, 1H), 8.78 (s, 1H), 8.27 (s, 1H), 7.95 (s, 1H), 4.78 (d, $J = 5.7$ Hz, 4H), 3.22 (d, $J = 7.6$ Hz, 4H), 2.14 (s, 2H), 1.88 (d, $J = 5.7$ Hz, 4H), 1.50 (d, $J = 5.9$ Hz, 4H), 1.38 (d, $J = 3.8$ Hz, 4H), 1.27 (d, $J = 16.0$ Hz, 34H), 0.97 (s, 14H), 0.87 (d, $J = 6.6$ Hz, 12H), 0.67 (d, $J = 8.5$ Hz, 6H).

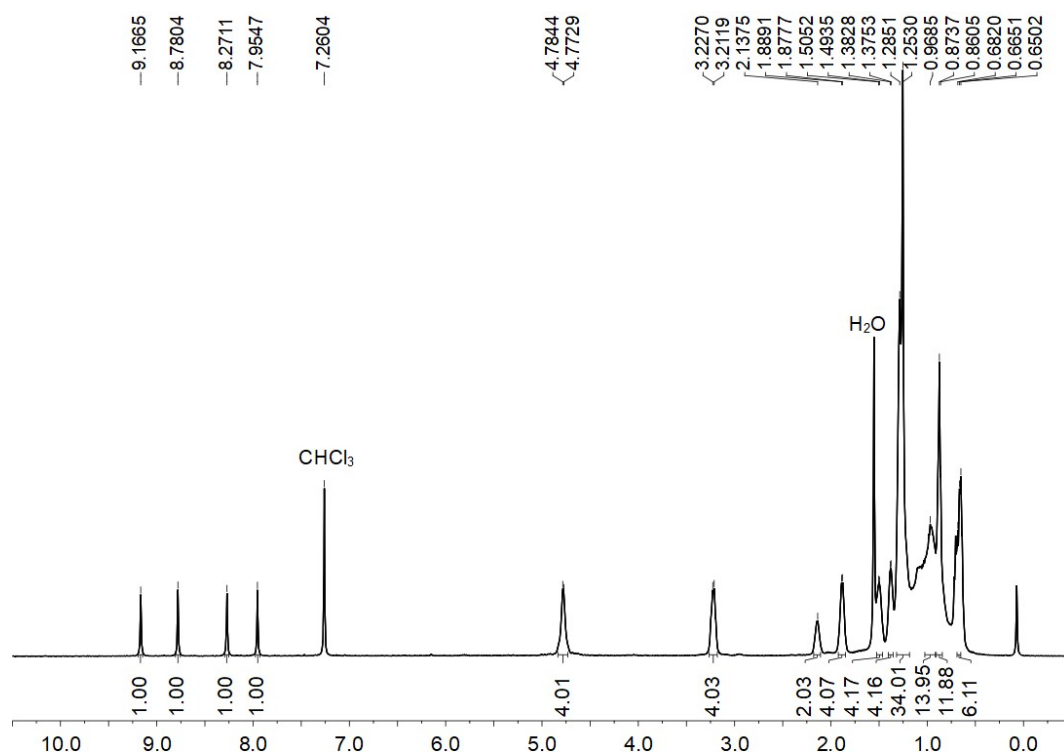
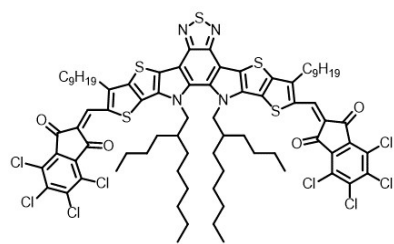


Fig. S1. ¹H NMR spectrum (500 MHz, CDCl₃, 298 K) of **BTP-TCID-2CN**.

2.2 Synthesis of **BTP-2TCID**



BTP-2TCID was synthesized according to literature procedure.¹ ¹H NMR (500 MHz, CDCl₃, 298K) δ (ppm): 8.27 (s, 2H), 4.79 (d, J = 8.5 Hz, 4H), 3.21 (d, J = 15.3 Hz, 4H), 2.15 (s, 2H), 1.89 (s, 4H), 1.49 (s, 4H), 1.38 (s, 4H), 1.27 (d, J = 17.1 Hz, 34H), 1.07–0.92 (m, 14H), 0.88 (d, J = 6.4 Hz, 6H), 0.69 (d, J = 27.7 Hz, 12H).

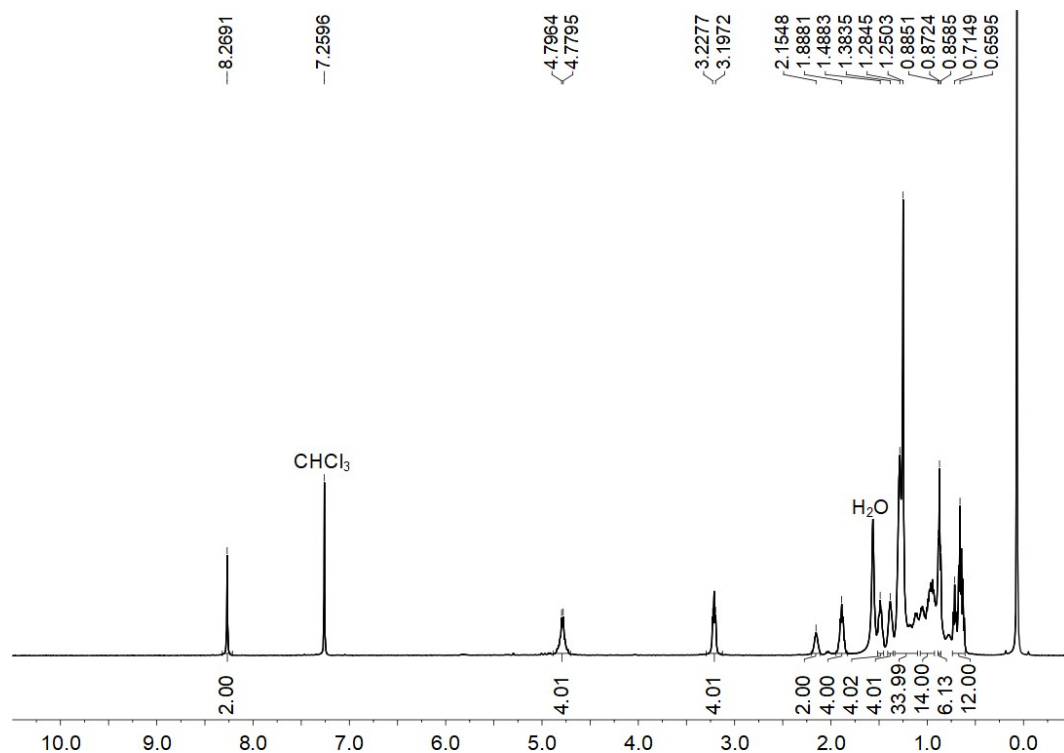


Fig. S2. ¹H NMR spectrum (500 MHz, CDCl₃, 298 K) of **BTP-2TCID**.

3. Theoretical calculation

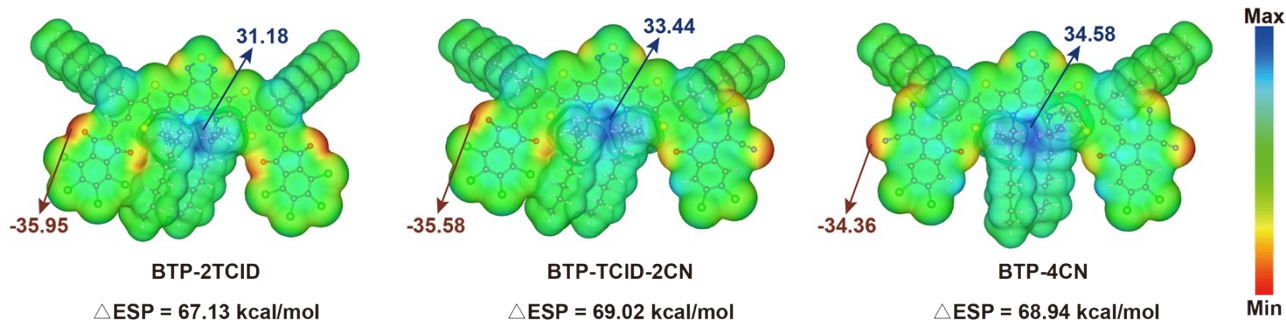


Fig. S3. ESP distributions of **BTP-2TCID**, **BTP-TCID-2CN** and **BTP-4CN**

4. Fabrication and characteristic of nanoparticles

Fabrication of BTP-2TCID NPs, BTP-TCID-2CN NPs and BTP-4CN NPs. The nanoparticles (NPs) were prepared by nanoprecipitation. Firstly, 1.5 mg **BTP-2TCID** was dissolved in 1.0 mL THF and 10.0 mg F127 was dissolved in

deionized water, respectively. Then the THF solution was dropped into the aqueous solution of F127 slowly, and the mixture was stirred at room temperature overnight. After evaporation of THF, the **BTP-2TCID** NPs solution was obtained and further concentrated under the low temperature and pressure for use. **BTP-TCID-2CN** NPs and **BTP-4CN** NPs were fabricated according to the identical process.

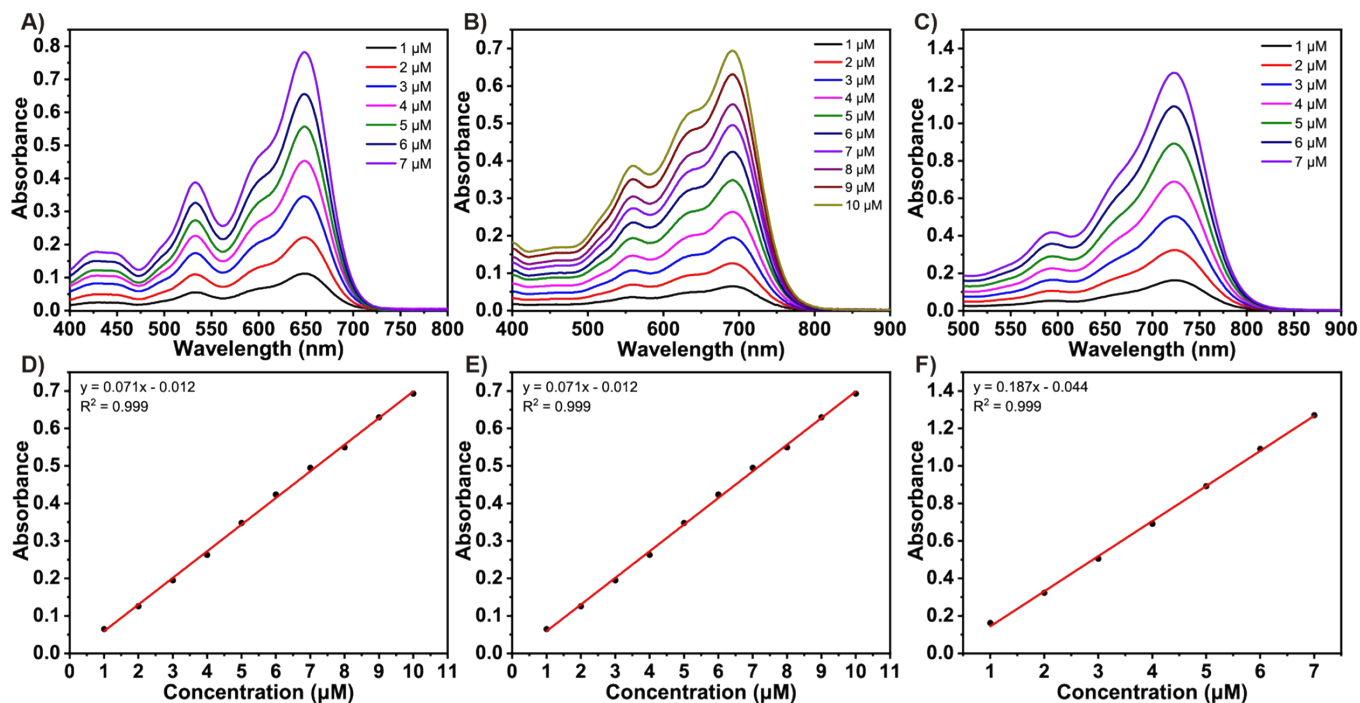


Fig. S4. UV-vis absorption spectra of A) **BTP-2TCID**, B) **BTP-TCID-2CN** and C) **BTP-4CN**. Standard curves of D) **BTP-2TCID**, E) **BTP-TCID-2CN** and F) **BTP-4CN** at various concentrations.

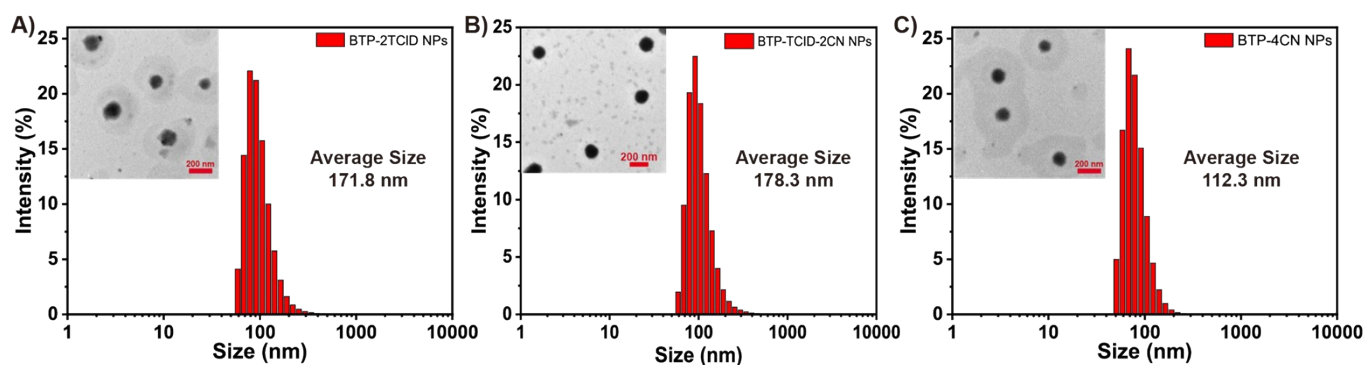


Fig. S5. DLS and TEM (inset) of A) **BTP-2TCID** NPs, B) **BTP-TCID-2CN** NPs and C) **BTP-4CN** NPs.

5. Verification J-aggregation of **BTP-2TCID** NPs, **BTP-TCID-2CN** NPs and **BTP-4CN** NPs

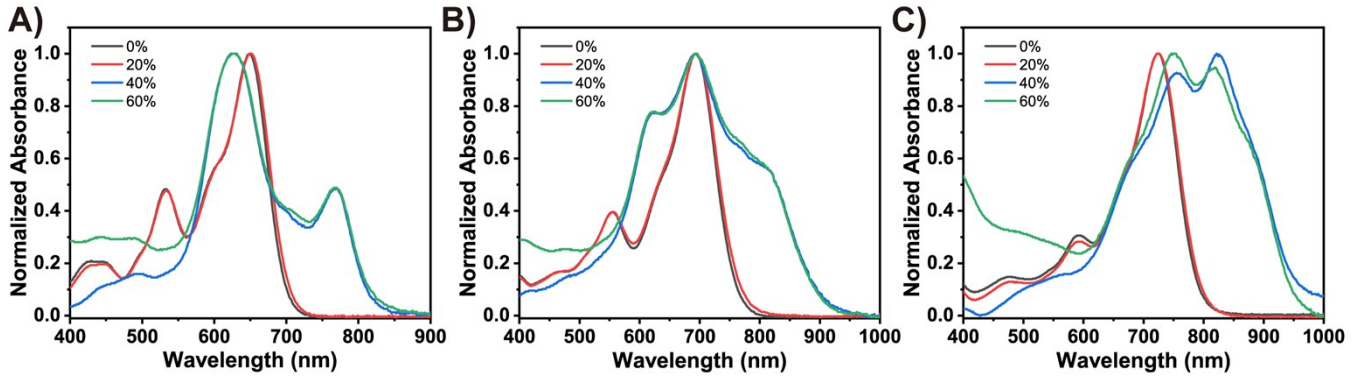


Fig. S6. UV-vis spectra of A) **BTP-2TCID** NPs, B) **BTP-TCID-2CN** NPs and C) **BTP-4CN** NPs in THF/water.

6. Photothermal performance of **BTP-2TCID** NPs, **BTP-TCID-2CN** NPs and **BTP-4CN** NPs

All solutions of **BTP-2TCID**, **BTP-TCID-2CN** and **BTP-4CN** NPs (20 $\mu\text{g/mL}$, 1.0 mL) were irradiated under 808 nm laser for 10 min, respectively. A FLIR thermal camera was used to record the temperature change.

Concentration-dependent photothermal property. **BTP-2TCID** NPs, **BTP-TCID-2CN** NPs and **BTP-4CN** NPs aqueous solutions of different concentrations (5, 10, 20, 40 $\mu\text{g/mL}$) were irradiated under 808 nm laser (1.0 W/cm^2) for 10 min, respectively. A FLIR thermal camera was used to record the temperature change.

Power density-dependent property. **BTP-2TCID** NPs, **BTP-TCID-2CN** NPs and **BTP-4CN** NPs aqueous solutions (20 $\mu\text{g/mL}$) were irradiated under 808 nm laser for 10 min under different power density (0.50, 0.75, 1.00, 1.25 W/cm^2), respectively. A FLIR thermal camera was used to record the temperature change.

Photothermal stability. **BTP-2TCID** NPs, **BTP-TCID-2CN** NPs and **BTP-4CN** NPs aqueous solutions (20 $\mu\text{g/mL}$) were irradiated under 808 nm laser (1.0 W/cm^2) for 10 min, then cooled down naturally for 20 min, respectively. This procedure was repeated for 4 times, and a FLIR thermal camera was used to record the temperature change.

Calculation of photothermal conversion efficiency. NPs aqueous solution (20 $\mu\text{g/mL}$) and deionized water were irradiated under 808 nm laser (1.0 W/cm^2) for 10 min and then cooled down naturally. Deionized water was used as control. The photothermal conversion efficiency (η) was calculated according to the following equations:

$$\eta = \frac{hS(T_{max} - T_0) - Q_{dis}}{I(1 - 10^{-A})}$$

T_{max} is the maximum temperature of the sample at the jarless state; T_0 is the initial temperature of the sample; Q_{dis} expresses the dissipation of heat; I is the laser power; A is the absorbance of sample at 808 nm.

hS is obtained from the following equation:

$$hS = \frac{m_D c_D}{\tau_s}$$

m_D is the mass of the solution (1.0 g); c_D is the particular heat capacity of the solution; τ_s is a time constant of the solution which can be calculated by the following equation:

$$\tau_s = - \frac{t}{\ln\left(\frac{T_{surr} - T}{T_{surr} - T_{max}}\right)}$$

T_{surr} is surrounding temperature; T is real-time temperature of the sample.

Q_{dis} is determined by the following equation:

$$Q_{dis} = \frac{m_D c_D (T_{max, water} - T_{surr})}{\tau_{water}}$$

$T_{max, water}$ is the maximum temperature of the water at the jarless state; τ_{water} is the time constant of the control group.

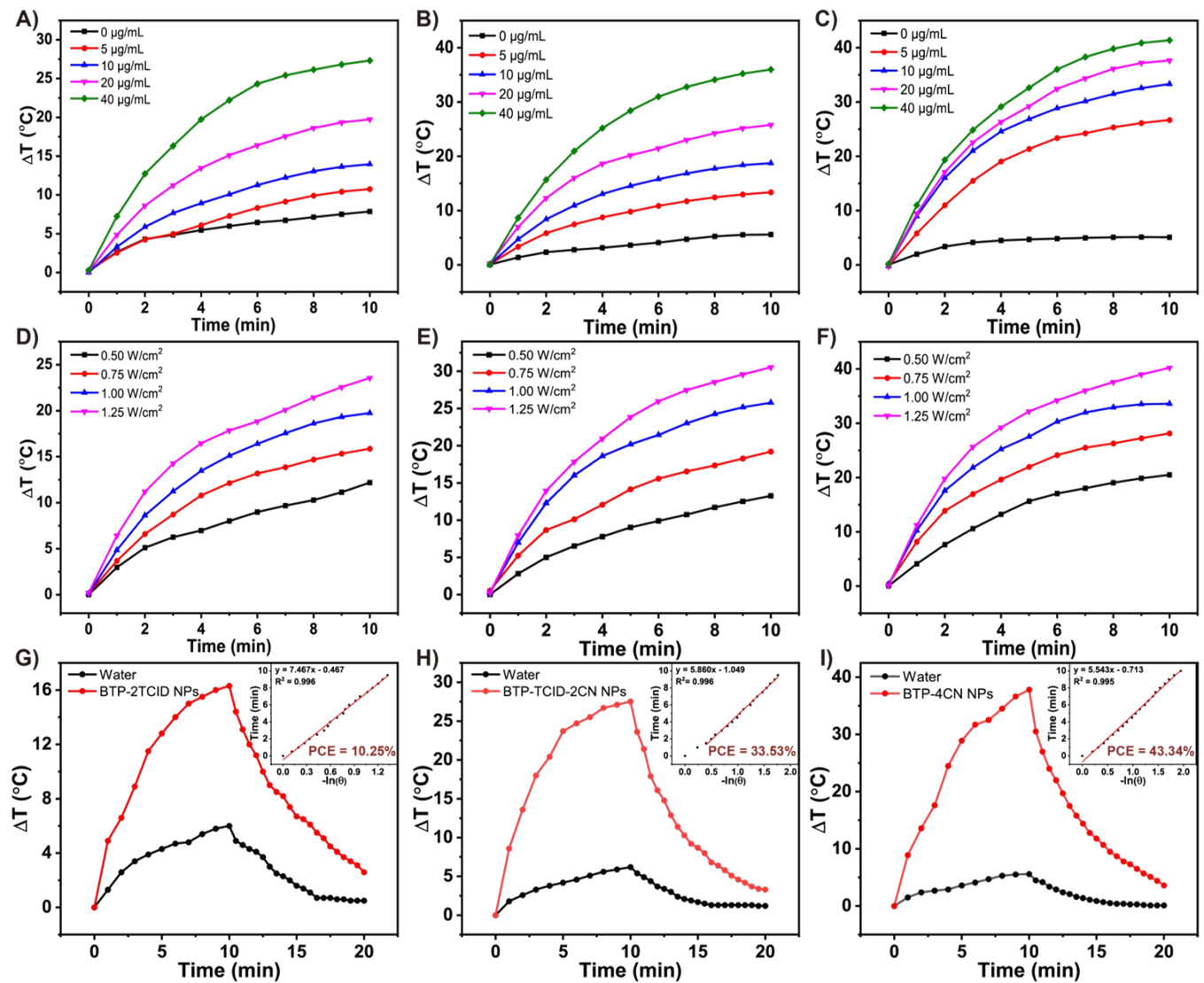


Fig. S7. Temperature curves under 808 nm laser irradiation (1.0 W/cm^2) for 10 min with different concentrations of A) BTP-

2TCID NPs, B) **BTP-TCID-2CN** NPs and C) **BTP-4CN** NPs. Temperature curves under 808 nm laser irradiation for 10 min with different power densities of D) **BTP-2TCID** NPs, E) **BTP-TCID-2CN** NPs and F) **BTP-4CN** NPs (20 µg/mL). Photothermal conversion efficiency of G) **BTP-2TCID** NPs, H) **BTP-TCID-2CN** NPs and I) **BTP-4CN** NPs under 808 nm irradiation for 10 min, then cooling down. Inset: Time versus the negative natural logarithm of the temperature in the cooling process of the different NPs.

7. Photodynamic properties of NPs

1,3-Diphenylisobenzofuran (DPBF) was added into the solution of different NPs as a probe, and all solutions of **BTP-2TCID** NPs, **BTP-TCID-2CN** NPs and **BTP-4CN** NPs were irradiated under 808 nm laser, respectively. Evaluate the ROS generation ability by recording the absorbance at 417 nm.

Concentration-dependent photodynamic property. **BTP-2TCID** NPs, **BTP-TCID-2CN** NPs and **BTP-4CN** NPs aqueous solutions of different concentrations (0.1, 1.0, 2.0 µg/mL) were irradiated by 808 nm laser (1.0 W/cm²), respectively. Evaluate the ROS generation ability by recording the absorbance at 417 nm.

Power density-dependent property. **BTP-2TCID** NPs, **BTP-TCID-2CN** NPs and **BTP-4CN** NPs aqueous solutions (2.0 µg/mL) were irradiated under 808 nm laser with different power densities (0.25, 0.50, 1.00 W/cm²), respectively. Evaluate the ROS generation ability by recording the absorbance at 417 nm.

Determination of photodynamic type. The species of ROS can be qualitatively detected by ESR spectrometer. 5,5-Dimethyl-1-pyrroline-1-oxide (DMPO) was used as a spin capturer to test the ·OH and O₂^{·-} radicals, and 2,2,6,6-tetramethylpiperidine (TEMP) to test ¹O₂.

Calculation of ROS generation quantum yield. The NPs aqueous solution (2.0 µg/mL) and ICG aqueous solution were irradiated under 808 nm laser (1.0 W/cm²) for 50 s and DPBF was added into the solution as a probe. Then the absorbance at 417 nm was recorded every 5 s. ICG aqueous solution was used as a control substance. The ROS generation quantum yield (Φ) was calculated according to the following equations:

$$\Phi = \Phi_{ICG} \times \frac{k}{k_{ICG}} \times \frac{F_{ICG}}{F}$$

Φ_{ICG} is the ¹O₂ generation quantum yield of ICG; k and k_{ICG} is the slope of time versus absorbance, respectively.

F is obtained from the following equation:

$$F = 1 - 10^{-abs}$$

The abs is the absorbance at 808 nm.

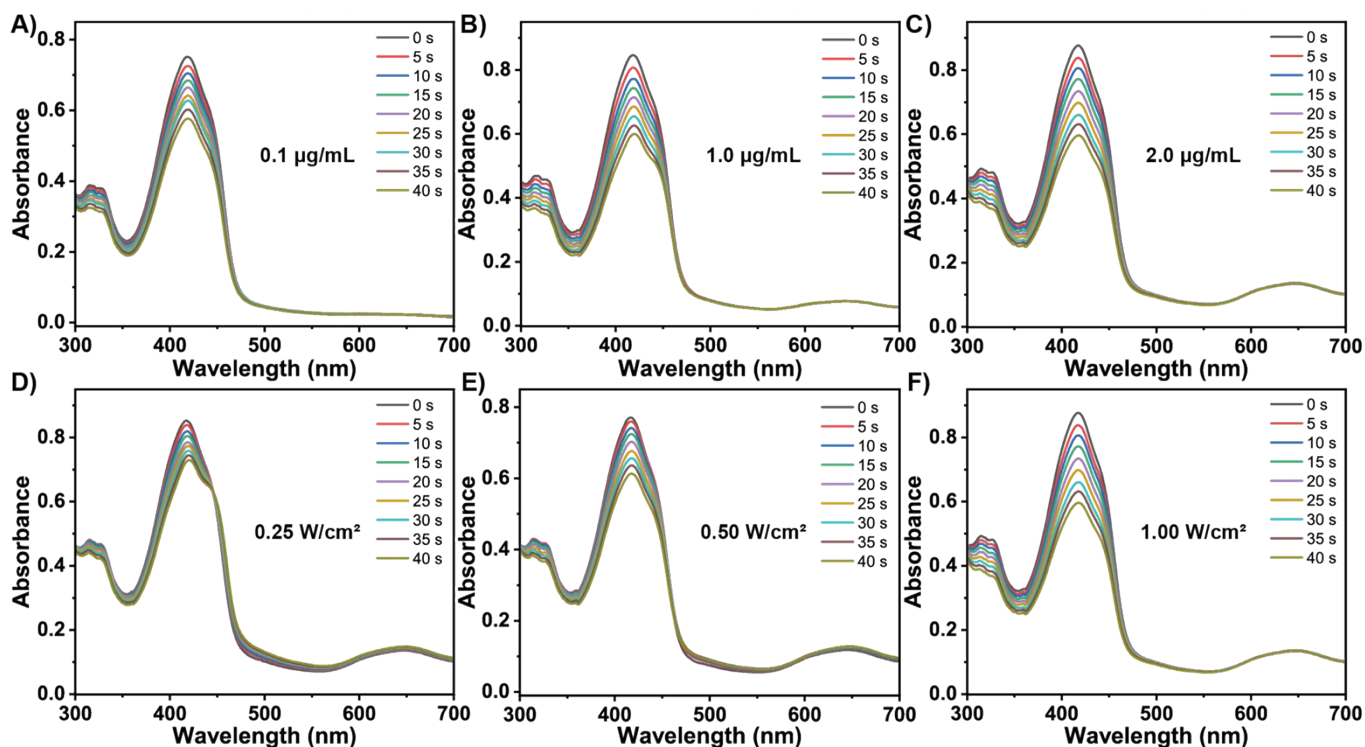


Fig. S8. Real-time UV-vis absorption spectra of DPBF (at 417 nm) along with 808 nm laser irradiation (1.0 W/cm^2) in the presence of A) $0.1 \text{ }\mu\text{g/mL}$, B) $1.0 \text{ }\mu\text{g/mL}$ and C) $2.0 \text{ }\mu\text{g/mL}$ of **BTP-2TCID** NPs in deionized water. Real-time UV-vis absorption spectra of DPBF (at 417 nm) under 808 nm laser irradiation in the different power of D) 0.25 W/cm^2 , E) 0.50 W/cm^2 and F) 1.00 W/cm^2 in the presence of **BTP-2TCID** NPs ($2.0 \text{ }\mu\text{g/mL}$) in deionized water.

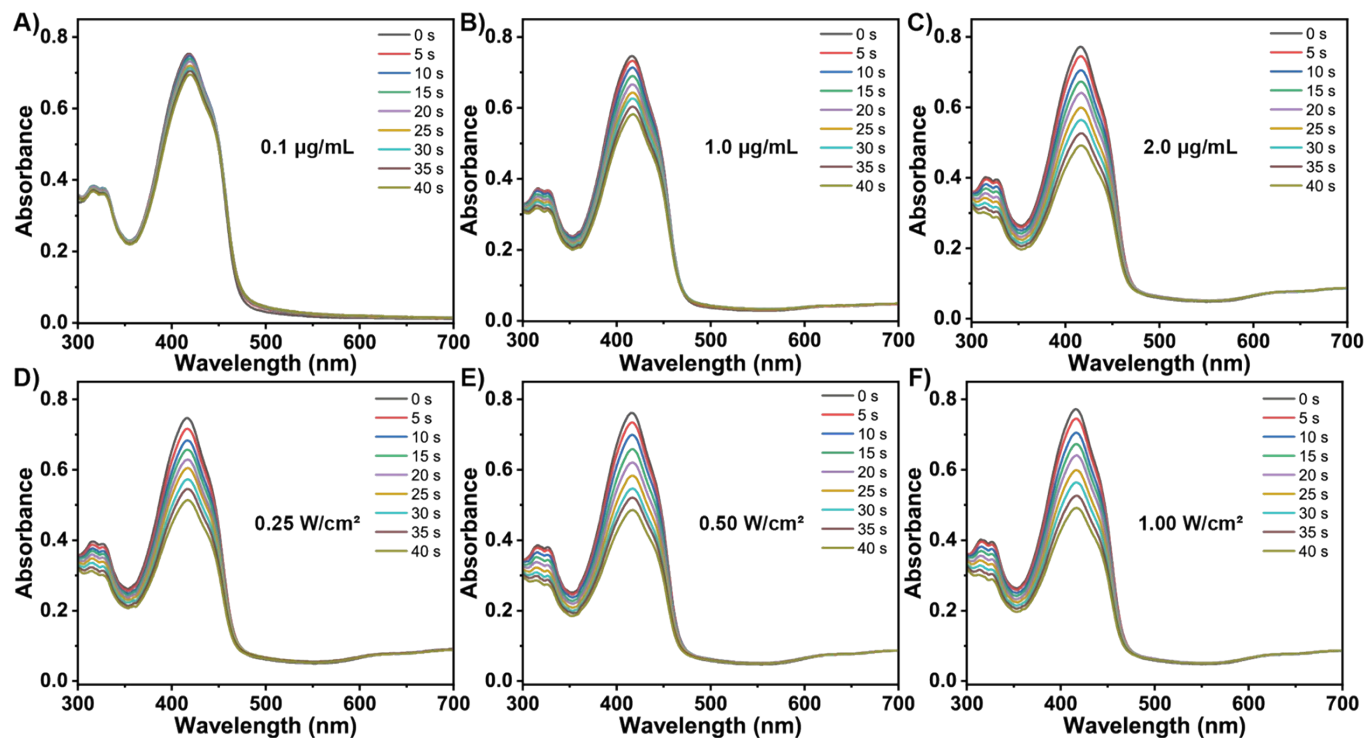


Fig. S9. Real-time UV-vis absorption spectra of DPBF (at 417 nm) along with 808 nm laser irradiation (1.0 W/cm^2) in the presence of A) $0.1 \text{ }\mu\text{g/mL}$, B) $1.0 \text{ }\mu\text{g/mL}$ and C) $2.0 \text{ }\mu\text{g/mL}$ of **BTP-TCID-2CN** NPs in deionized water. Real-time UV-vis absorption spectra of DPBF (at 417 nm) under 808 nm laser irradiation in the different power of D) 0.25 W/cm^2 , E) 0.50 W/cm^2

and F) 1.00 W/cm² in the presence of **BTP-TCID-2CN** NPs (2.0 μg/mL) in deionized water.

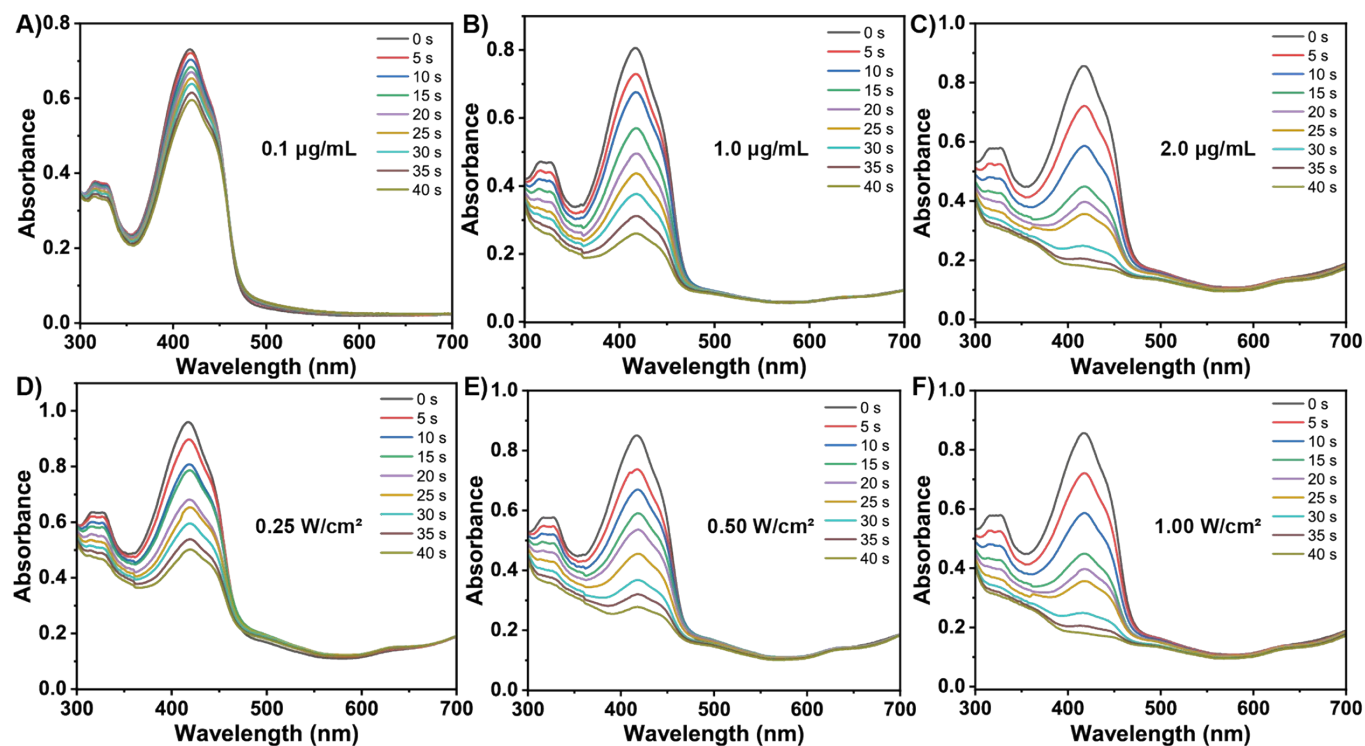


Fig. S10. Real-time UV-vis absorption spectra of DPBF (at 417 nm) under 808 nm laser irradiation (1.0 W/cm²) in the presence of A) 0.1 μg/mL, B) 1.0 μg/mL and C) 2.0 μg/mL of **BTP-4CN** NPs in deionized water. Real-time UV-vis absorption spectra of DPBF (at 417 nm) under 808 nm laser irradiation in the different power of D) 0.25 W/cm², E) 0.50 W/cm² and F) 1.00 W/cm² in the presence of **BTP-4CN** NPs (2.0 μg/mL) in deionized water.

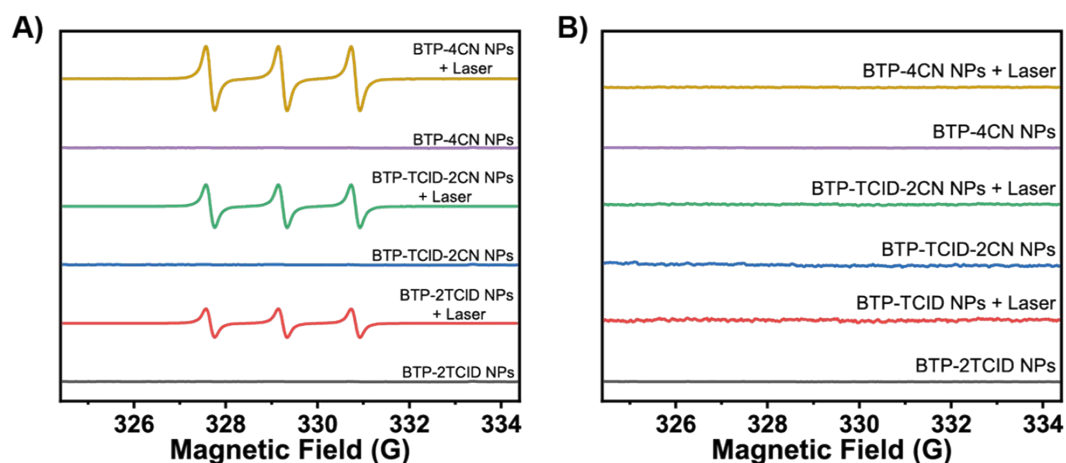


Fig. S11. EPR signals of different NPs. A) TEMP for ¹O₂ detection, and B) DMPO for ·OH detection.

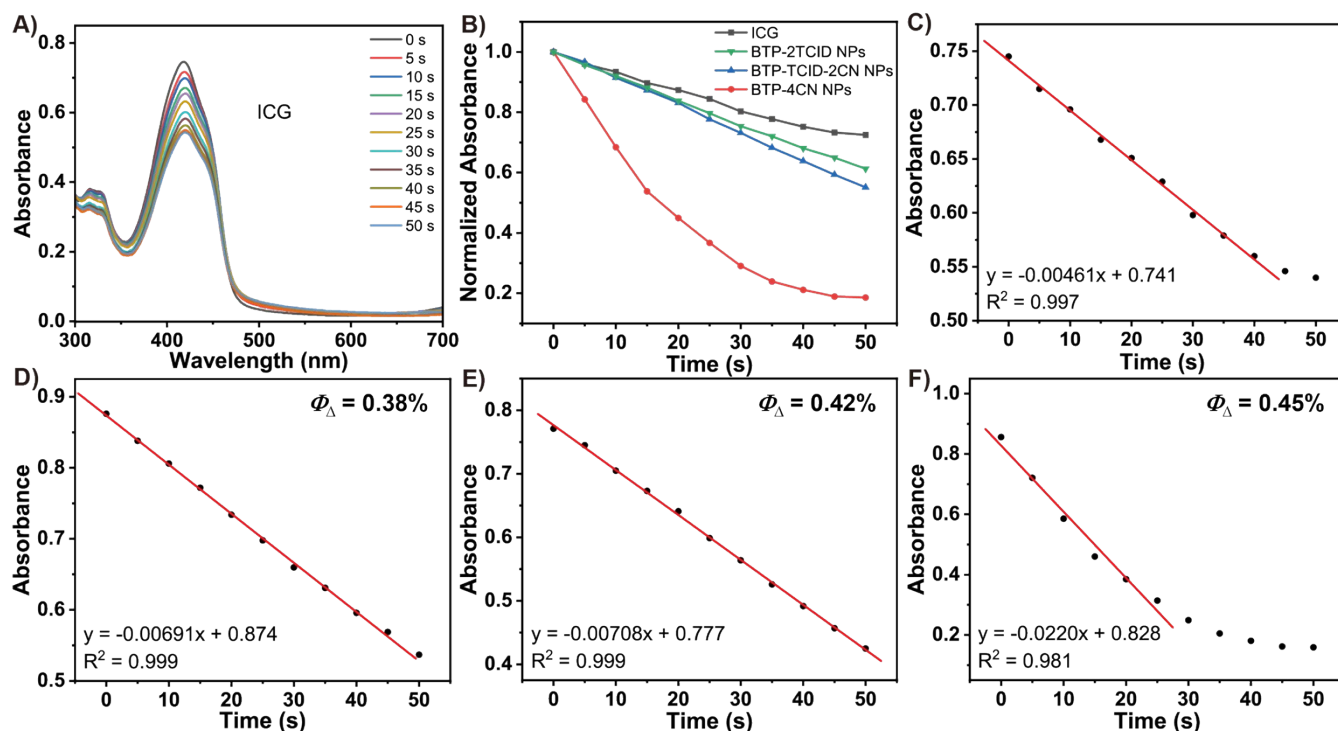


Fig. S12. A) Real-time UV-vis absorption spectra of DPBF (at 417 nm) along with 808 nm laser irradiation (1.0 W/cm²) in the presence of 2.0 µg/mL of ICG in deionized water. B) ROS generation from ICG and different NPs (2.0 µg/mL) with DPBF under 808 nm laser irradiation (1.0 W/cm²), respectively. Plot of absorbance vs the irradiation time of C) ICG, D) **BTP-2TCID** NPs, E) **BTP-TCID-2CN** NPs and F) **BTP-4CN** NPs, respectively.

8. Cell culture

The mouse glioma cells U87 were cultured in Dulbecco's modified Eagle medium (DMEM) with 10% new-born calf serum, 1% penicillin and streptomycin in a 5% CO₂ humidified atmosphere at 37 °C.

9. Intracellular uptake

The intracellular uptake was evaluated by confocal laser scanning microscopy (CLSM). U87 cells were incubated in 24-well plate at a density of 4×10⁴ cells/well. After incubation for 16 h, the medium was replaced by the fresh DMEM with **BTP-4CN** or **BTP-TCID-2CN** or **BTP-2TCID** NPs at the concentration of 200 ng/mL, respectively. After 4 h of incubation, the medium were removed and washed twice with DMEM (phenol red-free), anchored by 4% formaldehyde for 10 min. Then 4',6-diamidino-2-phenylindole (DAPI, 500 µL/well) was used to stain nucleus. After 10 min of dyeing, cells were washed twice with DMEM (phenol red-free) and imaged with CLSM.

10. MTT assay

The cell viability of **BTP-2TCID** NPs, **BTP-TCID-2CN** NPs and **BTP-4CN** NPs was evaluated by MTT assay,

respectively. U87 cells were inoculated in 96-well plate at 1×10^4 cells/well for 16 h, then substituted the medium by the fresh DMEM with **BTP-2TCID** or **BTP-TCID-2CN** or **BTP-4CN** NPs at different concentrations, respectively. After incubation for 4 h, some wells were exposed under 808 nm laser (1.0 W/cm^2) for 5 min, and others were kept without laser. After incubation for another 24 h, cells were determined by MTT assay with an enzyme microplate reader (DNM-9602, Perlong).

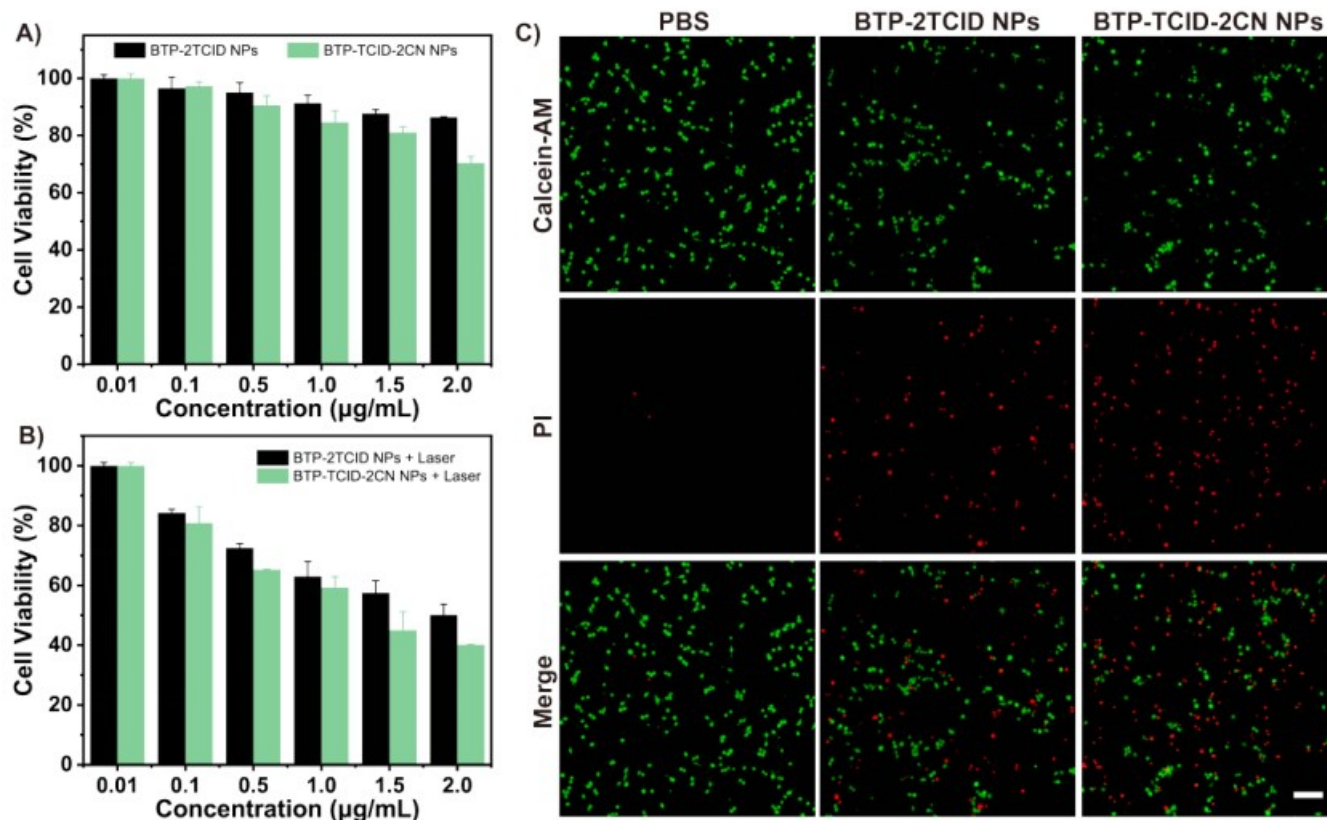


Fig. S13. A) Dark-toxicity and B) phototoxicity of **BTP-2TCID** NPs and **BTP-TCID-2CN** NPs. C) Live/dead assay of U87 cells treated with different NPs (2.0 µg/mL) with 808 nm irradiation (1.0 W/cm^2). Scale bars: 50 µm .

11. ROS detection in vitro

Intracellular ROS generation was detected by 2',7'-dichlorodihydrofluorescein diacetate (DCFH-DA) as an indicator. Following incubation with DMEM (phenol red-free), **BTP-2TCID** NPs (200 ng/mL), **BTP-TCID-2CN** NPs (200 ng/mL) and **BTP-4CN** NPs (200 ng/mL) for 4 h, DCFH-DA (10 µM) was loaded into the cells. After 20 min cultivation, cells were washed twice with DMEM (phenol red-free), and then treated with or without 808 nm laser (1.0 W/cm^2 , 10 s). The fluorescence images were obtained by CLSM.

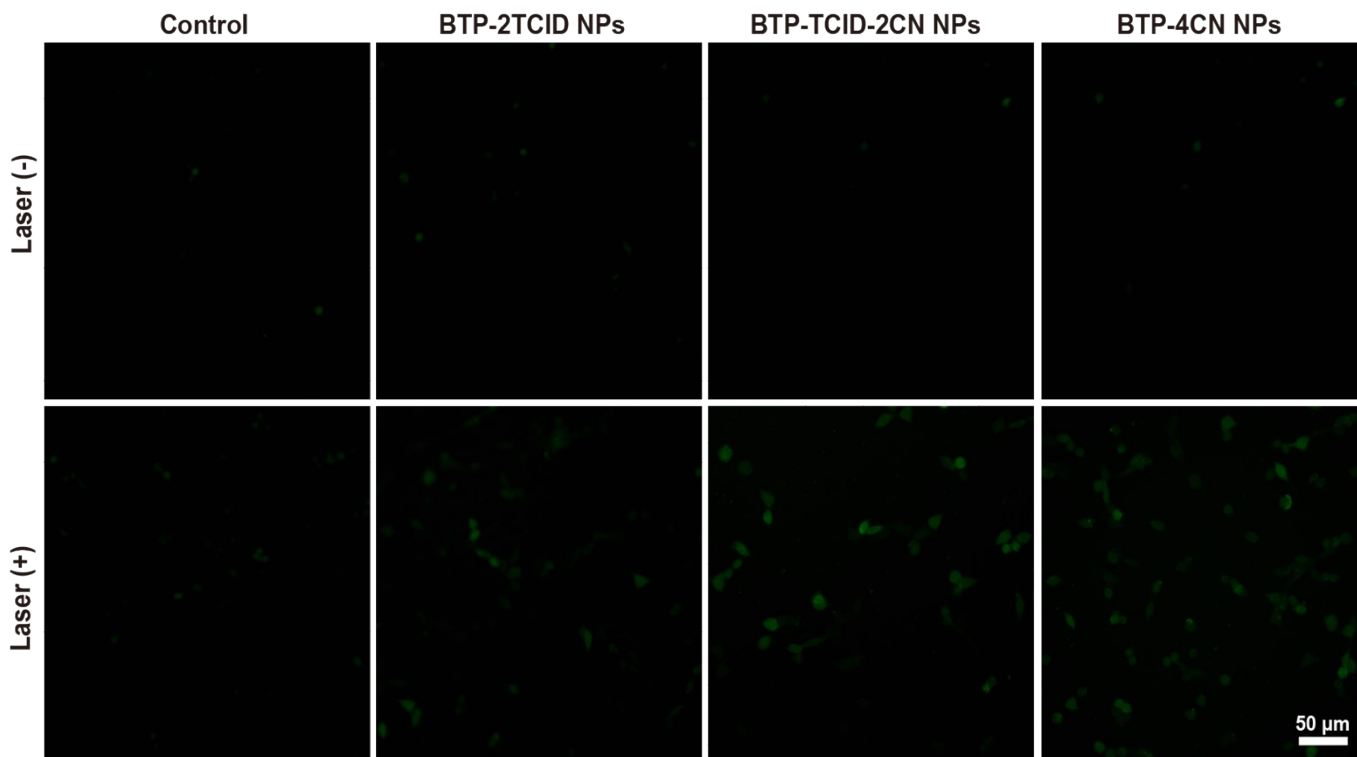


Fig. S14. ROS detection on U87 cells with different NPs by using DCFH-DA as an indicator, respectively.

12. Live/dead cell staining assay

Live/dead cell staining assay was detected by calcein acetoxymethyl ester (calcein AM) and propidium iodide (PI). U87 cells were seeded in 24-well plate at a density of 4×10^4 cells/well and cultured for 16 h. Then the medium was replaced by the fresh DMEM, **BTP-2TCID** NPs (500 ng/mL), **BTP-TCID-2CN** NPs (500 ng/mL) and **BTP-4CN** NPs (500 ng/mL). After 4 h, light groups were applied to 808 nm laser irradiation (1.0 W/cm^2) for 5 min, and others were kept without laser. After further incubation for 24 h, the cells were washed twice by DMEM (phenol red-free), treated by Calcein AM and PI for 30 min, then washed the residual dyes for two times. The fluorescence images were obtained by CLSM, which green fluorescence of Calcein AM and red fluorescence of PI indicated live and dead cells, respectively.

13. Flow cytometry

The cell uptake ability were further evaluated by flow cytometry. U87 cells were cultured in 12-well plates at a density of 8×10^4 cells/well. After 16 h, the medium was replaced by the fresh DMEM with 200 ng/mL **BTP-4CN**, **BTP-TCID-2CN**, **BTP-2TCID** NPs at different time points (1, 2, 4, 6, 8 h), respectively. Finally, the cells were collected and washed twice by DMEM (phenol red-free), and the uptake capacity of the cells at different incubation time was compared by flow cytometry.

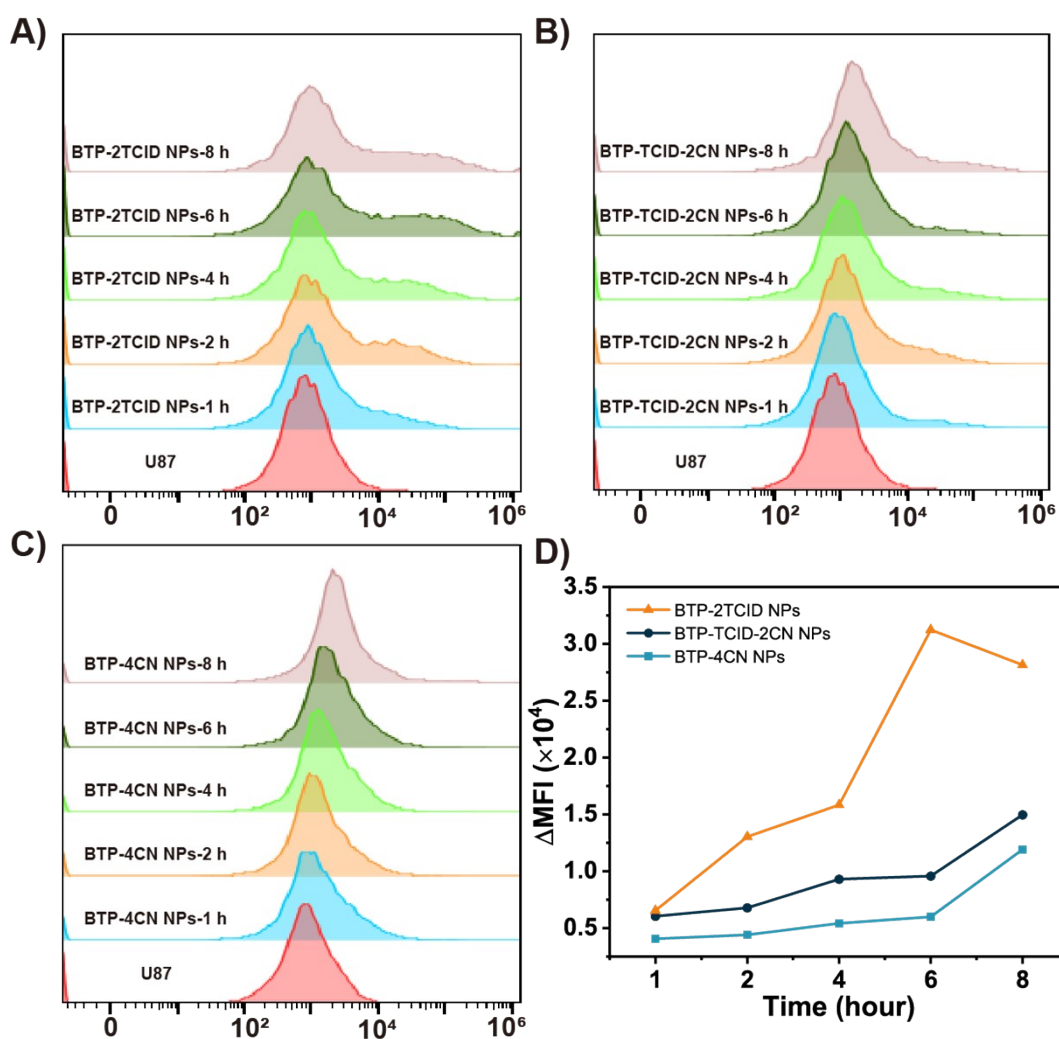


Fig. S15. Cell Uptake of U87 cells with A) **BTP-2TCID NPs**, B) **BTP-TCID-2CN NPs** and C) **BTP-4CN NPs** by flow cytometry at different time, respectively. D) Time-varying changes of mean fluorescence intensity (MFI) of U87 cells with different NPs.

14. Animal model

Female BALB/c nude mice (6 weeks old, weighting about 9-15 g) were purchased from Charles River Laboratory China Branch (Zhejiang, China) with production license number SCXK (Zhejiang) 2019-0001 and certificate number 20211228Abzz0619072327. The mice were housed at the Laboratory Animal Center of Hangzhou Normal University with use license number SYXK (Zhejiang) 2020-0026, and cultivated in a pathogen-free environment with appropriate humidity and temperature. All the conducted animal experiments were permitted by the Institutional Animal Care and Use Committee. Tumor-bearing mice were prepared by subcutaneously injection of 100 μ L of 10^6 U87 single cell suspension in PBS into the back of nude mice. After 6 days, the mice bearing U87 tumors with an average volume of ~ 80 mm³ were treated by **BTP-TCID-2CN NPs** *via* intratumor injection to explore the therapeutic effect.

15. Photothermal imaging

U87 tumor-bearing mice injected with NPs solution (20 $\mu\text{g}/\text{mL}$, 100 μL) was irradiated by 808 nm laser (1.0 W/cm^2) for 10 min, and the temperature of tumor was recorded by a FLIR thermal camera.

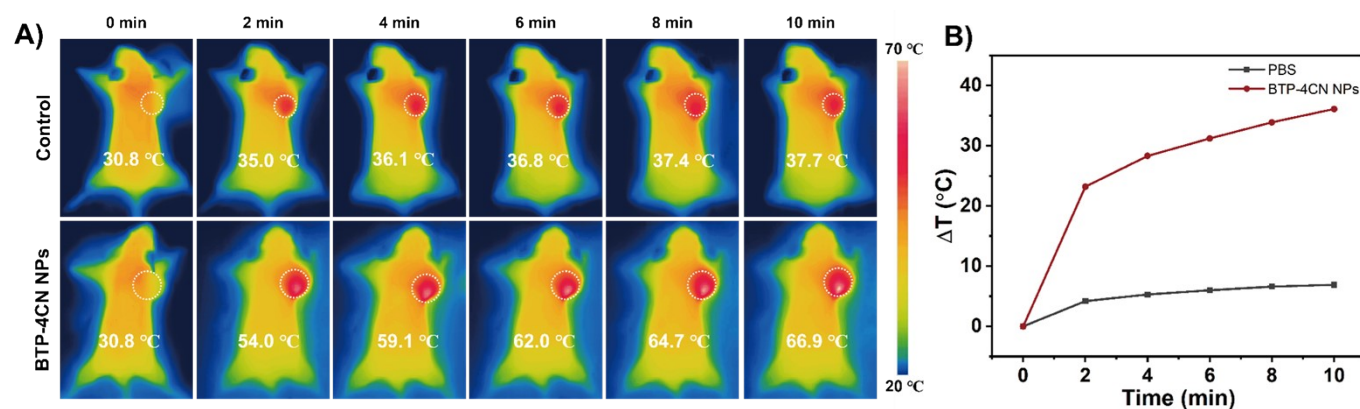


Fig. S16. A) Infrared thermal images of U87 tumor-bearing mice injected with 20 $\mu\text{g}/\text{mL}$ BTP-4CN NPs and PBS irradiated by 808 nm laser (1.0 W/cm^2) recorded every two minutes, respectively. B) Corresponding temperature change of the tumor sites.

16. In vitro and in vivo fluorescence imaging

In vitro fluorescence imaging (FLI) of BTP-TCID-2CN NPs with different concentrations (0, 5, 10, 20, 40, 60 $\mu\text{g}/\text{mL}$) was investigated. *In vivo* FLI of U87 tumor-bearing mice were injected 20 $\mu\text{g}/\text{mL}$ BTP-TCID-2CN NPs solution, which were detected using AniView100 multimodal animal imaging system.

17. In vitro and in vivo photoacoustic imaging

In vitro photoacoustic imaging (PAI) of BTP-TCID-2CN NPs with different concentrations (0, 10, 20, 40 $\mu\text{g}/\text{mL}$) was investigated. *In vivo* PAI of U87 tumor-bearing mice were injected with 20 $\mu\text{g}/\text{mL}$ BTP-TCID-2CN NPs, which were detected using MSOT.

18. In vivo anti-cancer therapy

In vivo anti-cancer therapy was performed using U87 tumor-bearing mice. The mice were randomly divided into 4 groups: I, only 100 μL PBS injection; II, 100 μL PBS injection and laser; III: 100 μL BTP-TCID-2CN NPs (20 $\mu\text{g}/\text{mL}$) injection; IV: 100 μL BTP-TCID-2CN NPs (20 $\mu\text{g}/\text{mL}$) injection and laser. The mice with laser group were exposed under 808 nm laser irradiation (1.0 W/cm^2) for 10 min. The treatments were conducted every two days. The mouse weight and tumor volume were measured every two days, and proceeded to the 18th day.

19. In vivo biological safe experiments

After tumour-bearing mice were sacrificed, tumors and major organs (heart, liver, spleen, lung and kidney) were dissected from the mice. The tissues were fixed in 4% paraformaldehyde, embedded paraffin and sectioned to slices with a thickness of 3 μm . The sections were subjected to haematoxylin and eosin (H&E), Ki67 and TUNEL staining for histopathological analysis. At the moment, eyeball blood of mice was collected by enucleation of mouse eyes before sacrificed for further blood biochemistry and haematology analysis. The observed indexes were alkaline phosphatase (ALP), aspartate aminotransferase (AST), alanine aminotransferase (ALT) and urea nitrogen (BUN), red blood cells (RBC), white blood cells (WBC), haemoglobin (HGB), blood routine levers of haematocrit (HCT), mean corpuscular volume (MCV), blood platelet (PLT), mean corpuscular haemoglobin concentration (MCHC), mean corpuscular haemoglobin (MCH), mean platelet volume (MPV), red cell distribution width (RDW-CV), lymphocyte (LYMPH%), neutrophil (NEUT%).

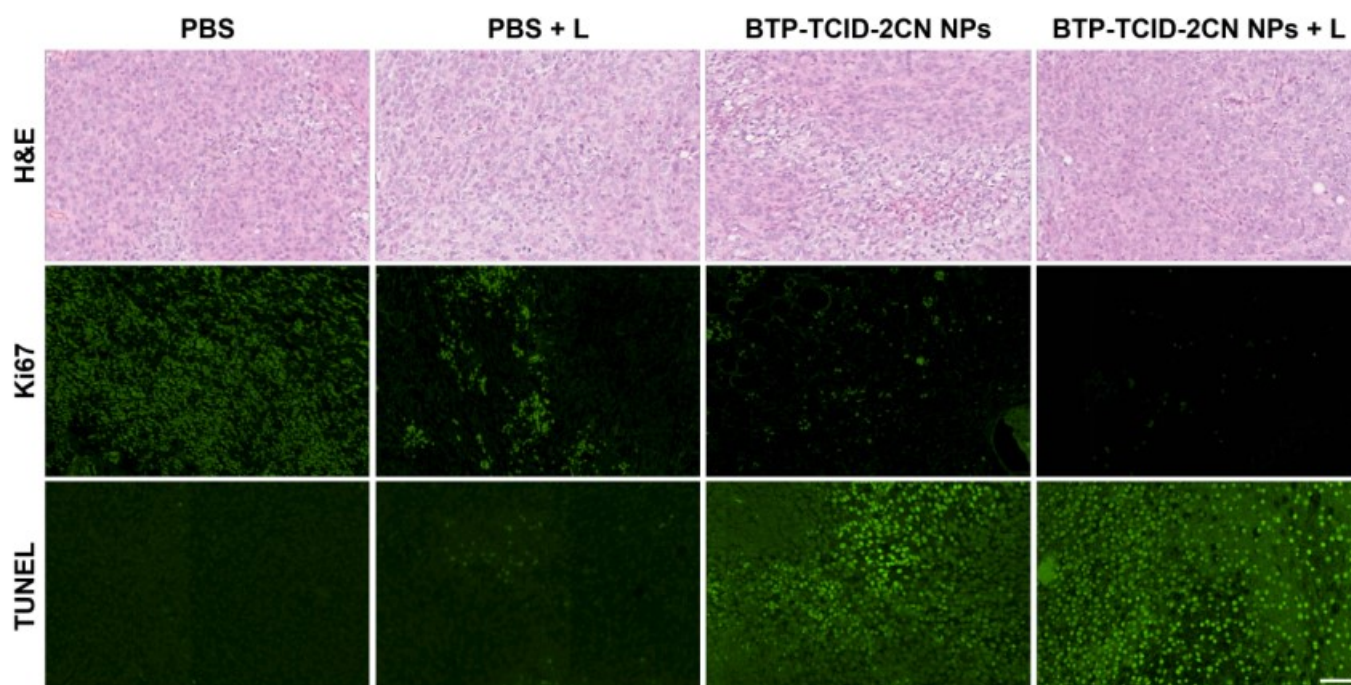


Fig. S17. H&E, Ki67 and TUNEL staining of tumor sections from U87 tumor-bearing mic, respectively. All the scale bars are 100 μm .

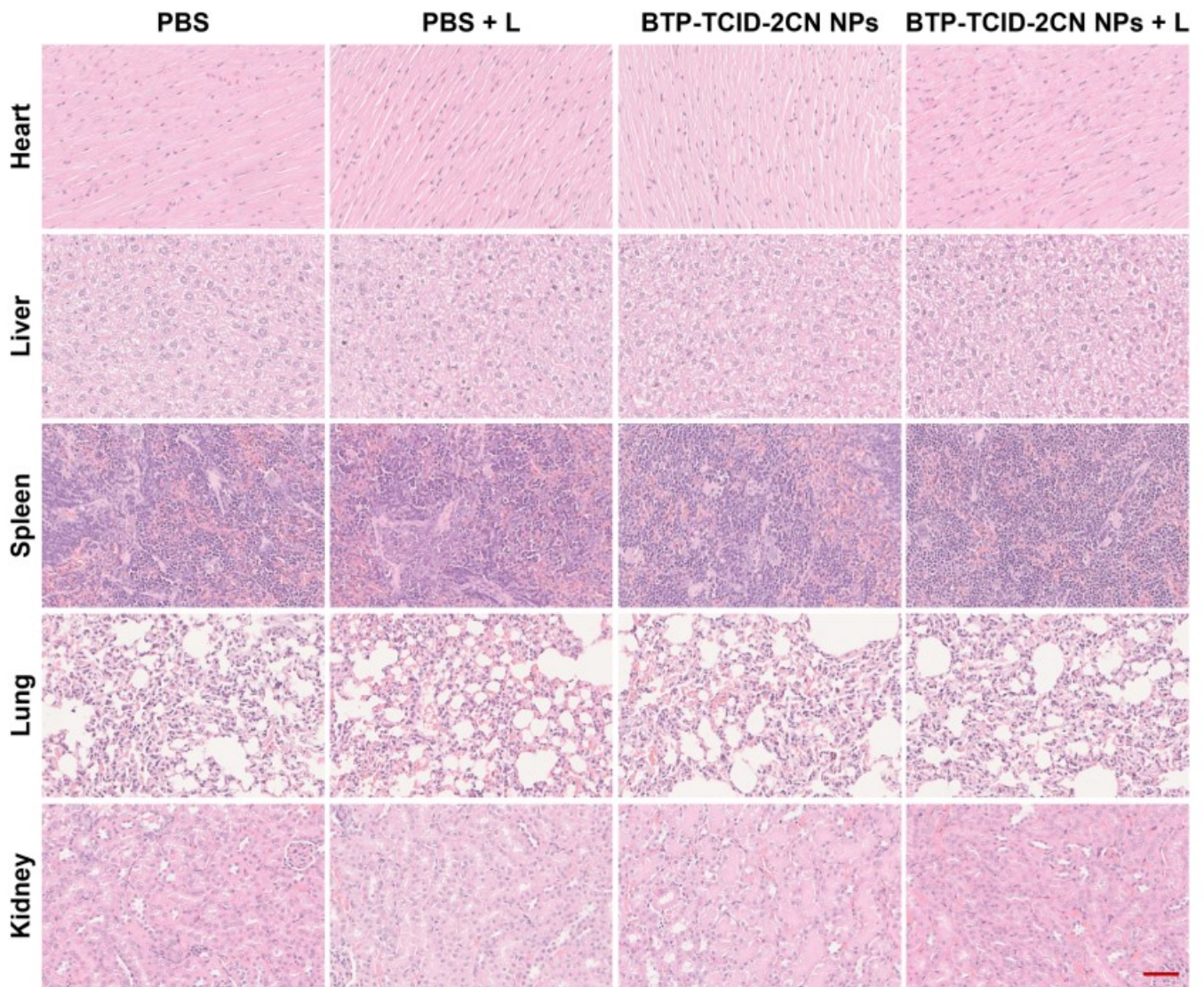


Fig. S18. H&E-stained tissue sections of major organs (heart, liver, spleen, lung, and kidney) of mice. All the scale bars are 100 μm .

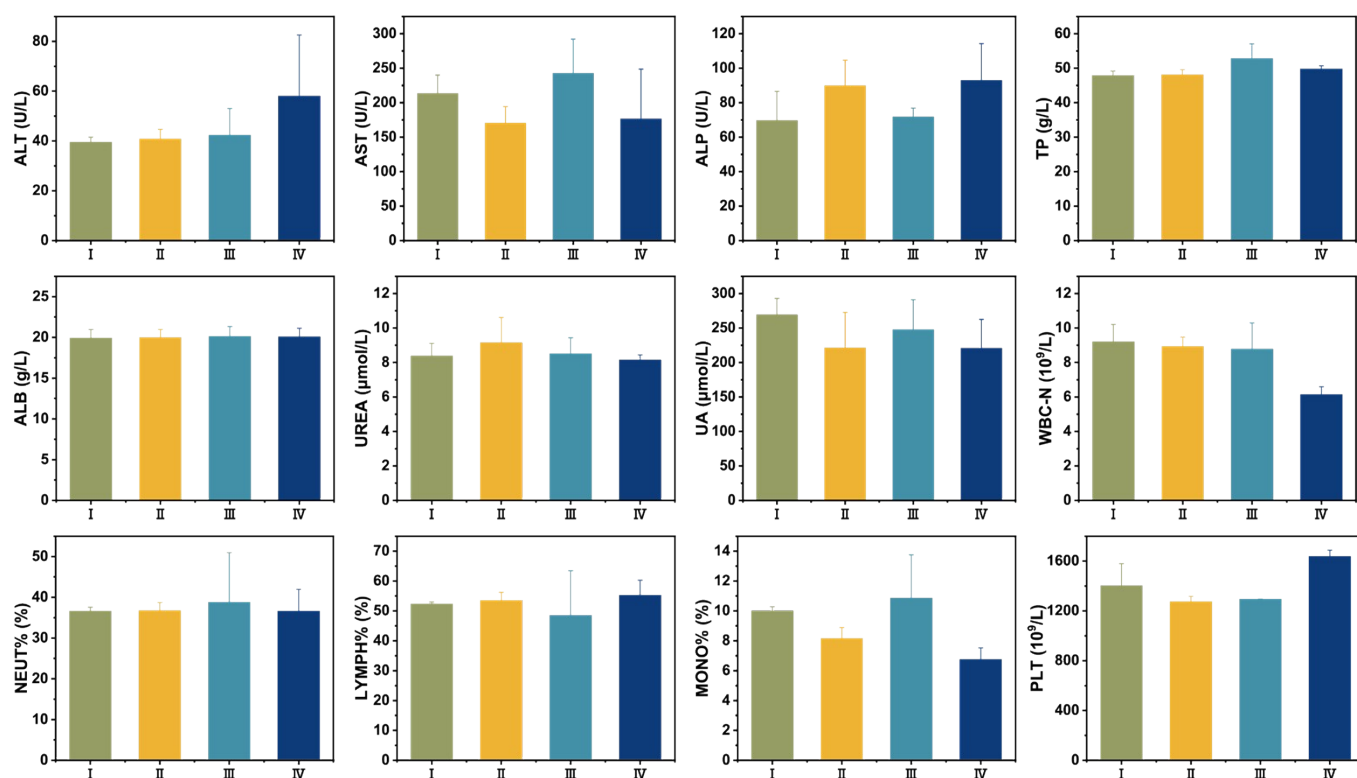


Fig. S19. The related indexes of blood biochemistry and hematology analysis from experimental mice after different treatments: I: PBS, II: PBS + Laser, III: **BTP-TCID-2CN NPs**, IV: **BTP-TCID-2CN NPs + Laser**.

20. Reference

- 1 L. Zhan, S. Li, Y. Li, R. Sun, J. Min, Y. Chen, J. Fang, C. Q. Ma, G. Zhou, H. Zhu, L. Zuo, H. Qiu, S. Yin, H. Chen, *Adv. Energy Mater.* **2022**, *12*, 2201076.